

SEARCHING FOR DEBRIS DISKS AROUND SEVEN RADIO PULSARS

ZHONGXIANG WANG¹, C.-Y. NG², XUEBING WANG^{1,3}, AIGEN LI⁴, DAVID L. KAPLAN⁵

Draft version August 18, 2018

ABSTRACT

We report on our searches for debris disks around seven relatively nearby radio pulsars, which are isolated sources and were carefully selected as the targets on the basis of our deep K_s -band imaging survey. The K_s images obtained with the 6.5 m Baade Magellan Telescope at Las Campanas Observatory are analyzed together with the *Spitzer*/IRAC images at 4.5 and 8.0 μm and the *WISE* images at 3.4, 4.6, 12 and 22 μm . No infrared (IR) counterparts of these pulsars are found, with flux upper limits of $\sim \mu\text{Jy}$ at near-infrared ($\lambda < 10 \mu\text{m}$) and $\sim 10\text{--}1000 \mu\text{Jy}$ at mid-infrared wavelengths ($\lambda > 10 \mu\text{m}$). The results of this search are discussed in terms of the efficiency of converting the pulsar spin-down energy to thermal energy and X-ray heating of debris disks, with comparison made to the two magnetars 4U 0142+61 and 1E 2259+586 which are suggested to harbor a debris disk.

Subject headings: infrared: stars — pulsars: individual (J0729–1448, B0740–28, J0940–5428, B0950+08, J1015–5719, J1317–5759, J1549–4848) — stars: neutron

1. INTRODUCTION

Disks are ubiquitous in astrophysical systems at all scales, found almost anywhere an axis of symmetry exists, and play an important role in the appearance and evolution of these systems. For example, they are essential for the creation of planetary systems, formation of young stars, mass-transfer in binary systems, and fueling of the central engines in active galactic nuclei, even though the physical properties of both the disks and their host systems differ dramatically.

Disks may also exist around isolated neutron stars, possibly formed from fallback material after supernova explosions (Lin et al. 1991; Chatterjee et al. 2000). When a massive star dies in a supernova explosion, some amount of the ejecta ($\leq 0.1M_\odot$) may “fallback” onto the newly formed neutron star (Chevalier 1989; Woosley & Weaver 1995). If much of the material is captured by the gravitational field of the neutron star and has sufficiently high angular momentum to prevent direct infall onto this compact star, a disk forms due to interactions between streams of the captured material.

There are a number of observational puzzles relating to radio pulsars that could be explained by disks (Michel & Dessler 1981; Cordes & Shannon 2008). The evolution of pulse periods with time for most pulsars does not actually follow the detailed predictions of magnetic dipole radiation (e.g., Livingstone et al. 2007; Espinoza et al. 2011), which could be due to disks (Menou et al. 2001; Çalişkan et al. 2013) exerting excess torque on the pulsars’ magnetospheres. In addition, some unique phenomena seen in individual pulsars, such as jets and neutron star precession, may arise from disks

(Blackman & Perna 2004; Qiao et al. 2003). The first extra-solar planet system was discovered around the radio pulsar B1257+12 (Wolszczan & Frail 1992). Even though the source is a millisecond pulsar with a complicated evolutionary path, it is generally believed that the planetary system had formed from a debris disk (e.g., Phinney & Hansen 1993; Miller & Hamilton 2001). There is a type of radio emitting neutron stars, called rotating radio transients (RRATs; McLaughlin et al. 2006), which are characterized by short, periodic radio bursts (2–30 ms) spaced by long intervals (ranging from minutes to hours). The bursts, along with other variations in radio pulses—such as pulse nulling, drifting subpulses, and mode changes, might be caused by dusty material from a surrounding debris disk falling into the magnetosphere of a pulsar (Cordes & Shannon 2008; Shannon et al. 2013).

Motivated by the discovery of the planetary system around PSR B1257+12, searches for debris disks around neutron stars have concentrated on old radio pulsars, but with no success (e.g. Foster & Fischer 1996; Koch-Miramond et al. 2002; Lazio & Fischer 2004). These searches were however limited by the choice of targets (older, less energetic pulsars) and the instrumentation (poor sensitivity and angular resolution). Multi-wavelength searches for fallback disks around a number of young neutron stars have been conducted (e.g., Wang et al. 2006, 2007a), although these are considered as high-energy objects, namely, central compact objects (CCOs; Pavlov et al. 2004; Gotthelf et al. 2013) and magnetars (Thompson & Duncan 1996), rather than ordinary/traditional radio pulsars. The former are a class of radio-quiet X-ray point sources at the centers of young supernova remnants while the latter are believed to generally have ultra-high surface magnetic fields ($\sim 10^{14}$ G; Woods & Thompson 2006).

Using the *Spitzer Space Telescope*, the infrared (IR) counterparts to the magnetars 4U 0142+61 and 1E 2259+586 have been found (Wang et al. 2006; Kaplan et al. 2009). For the former source, no single spectral model, such as a blackbody or a power

¹ Shanghai Astronomical Observatory, Chinese Academy of Sciences, 80 Nandan Road, Shanghai 200030, China

² Department of Physics, The University of Hong Kong, Pokfulam Road, Hong Kong

³ Graduate University of Chinese Academy of Sciences, Beijing 100049, China

⁴ Department of Physics and Astronomy, University of Missouri, Columbia, MO 65211, USA

⁵ Physics Department, University of Wisconsin-Milwaukee, Milwaukee, WI 53211, USA

law, can fit its combined optical and IR spectral energy distribution (SED). Instead, it is very likely that the IR emission arises from a residual dust disk. This disk, with estimated mass of $<10^{-3}M_{\odot}$, is heated by strong X-rays from the central pulsar ($L_X \simeq 10^{36}$ erg s^{-1}) and appears bright at IR wavelengths (for example, $L_{4.5\mu m} \simeq 5 \times 10^{31}$ ergs s^{-1}). The disk's lifetime was estimated to be $> 10^6$ yr, assuming that the magnetar has been spun down by mass accretion from the putative disk (Wang et al. 2006). The lifetime significantly exceeds the pulsar age ($\approx 10^5$ yr), suggesting a supernova fallback origin (Wang et al. 2006). While there were only K_s -band and *Spitzer* 4.5 μm detections of 1E 2259+586, the overall IR emission is similar to that of 4U 0142+61, suggesting the possible existence of a debris disk around this magnetar (Kaplan et al. 2009).

In order to explore the general existence of similar residual disks around isolated neutron stars, we have carried out disk searches around a few relatively young radio pulsars. The detectability of the disk around 4U 0142+61 is likely the result of a combination of the very strong X-ray heating of the disk and the relative youth of the object. For radio pulsars, their winds that carry much of their spin-down luminosity and contain energetic particles may heat a debris disk, producing IR emission (Jones 2007, 2008). Some fraction of the spin-down luminosity is conceivably assumed to illuminate surrounding disks.

In this paper we report the results of disk searches around seven relatively young pulsars from our ground-based and *Spitzer* observations. The pulsar targets were carefully selected partly on the basis of an initial near-IR K_s -band survey. Results from the all-sky survey conducted by the *Wide-field Infrared Survey Explorer* (*WISE*) were included. In addition, in order to understand the role of X-ray emission from neutron stars in disk heating (or disk detectability), X-ray flux values or upper limits of the seven pulsars, either from the literature or archival data analysis conducted by us, were also reported. Below we first describe our target selection in Section 1.1. The observations and data analysis are described in Section 2, and the results and discussion are presented in Sections 3 and 4, respectively.

1.1. Target Selection

We selected sources from the Pulsar Catalog⁶ (Manchester et al. 2005) based on the spin-down luminosity L_{sd} scaled by distance d , L_{sd}/d^2 , and picked the top 40 young, energetic pulsars that had not been well observed in the optical/IR bands. As one might expect near-IR emission from these systems if debris disks are present, we undertook observations in the K_s band using the 6.5-m Magellan telescopes (see Section 2). However, in no case did we find a near-IR counterpart.

Based on the ground-based observations, we then selected seven pulsars (see Table 1) as our targets for *Spitzer* observations. The reasons for the selection are the following. First, they are relatively nearby, with a typical distance of 4 kpc. A debris disk with temperature of approximately 1000 K (Wang et al. 2006) would be bright in the mid-IR at that distance. Second, these targets are not surrounded by synchrotron

nebulae that can envelope some of the most energetic pulsars (Kaspi et al. 2006; Gaensler & Slane 2006) and could hide mid-IR emission from the pulsar itself. Third and most important, since most pulsars are located primarily in the Galactic plane, the confusion with field stars is a serious problem. These targets were selected because they are in less crowded fields. Using the Galactic disk dust map (Schlegel et al. 1998), we estimated the extinction along each source's direction. The maximum extinction for our targets is approximately $A_V = 9$ (for three high Galactic latitude sources, they only have $A_V \approx 2$). This limits the extinction effect that could alter the apparent stellar colors and cause us to mistake it for a disk.

To our target selection we added one other source: RRAT J1317–5759. This object, which just emits sporadic bursts of radio waves, would not be detected simply based on our spin-down luminosity argument. However, the mechanism for the radio bursting is not clearly understood, and may be related to a surrounding debris disk (Cordes & Shannon 2008). Given that this source also has a clean field, we selected it as our target for testing this hypothesis.

2. OBSERVATIONS AND DATA REDUCTION

2.1. Magellan K_s -band Imaging

We observed the fields of the seven pulsar targets in the K_s band using Persson's Auxiliary Nasmyth Infrared Camera (PANIC; Martini et al. 2004) on the 6.5-m Baade Magellan Telescope at Las Campanas Observatory in Chile. The observation dates are provided in Table 2. The detector was a Rockwell Hawaii 1024 \times 1024 HgCdTe array, having a field of view (FOV) of 2' \times 2' and a pixel scale of 0.125'' pixel $^{-1}$. The total on-source exposure times were in a range of 13–30 min. During the exposure of a target, the telescope was dithered in a 3 \times 3 grid with offsets of 10'' to obtain a measurement of the sky background. The observing conditions were good, with 0''.4–0''.5 seeing in the K_s band. The FWHMs of point sources in our images are given in Table 2.

We used the IRAF data analysis package for data reduction. The images were bias-subtracted and flat-fielded. From each set of dithered images in one observation, a sky image was made by filtering out stars. The sky image was subtracted from the set of images, and then the sky-subtracted images were shifted and combined into one final image of a target field.

We astrometrically calibrated the images using the Two Micron All Sky Survey (2MASS; Skrutskie et al. 2006) stars detected in the fields. For the targets except B0950+08, 20–60 2MASS stars were used for the calibration, and the resulting uncertainties are of the order of 0''.03. Therefore, the positional uncertainties for locating the six pulsars on the images are dominated by the 2MASS systematic uncertainty of $\simeq 0''.15$. For B0950+08, only six 2MASS stars were detected to be used for the calibration, because it has a high Galactic latitude G_b . The nominal position uncertainty is 0''.13. Adding the 2MASS systematic uncertainty in quadrature, the positional uncertainty for locating it on the K_s image is 0''.2.

For flux calibration, 4–14 relatively bright 2MASS stars detected in the fields of the targets were used; bright

⁶ <http://www.atnf.csiro.au/people/pulsar/psrcat/>

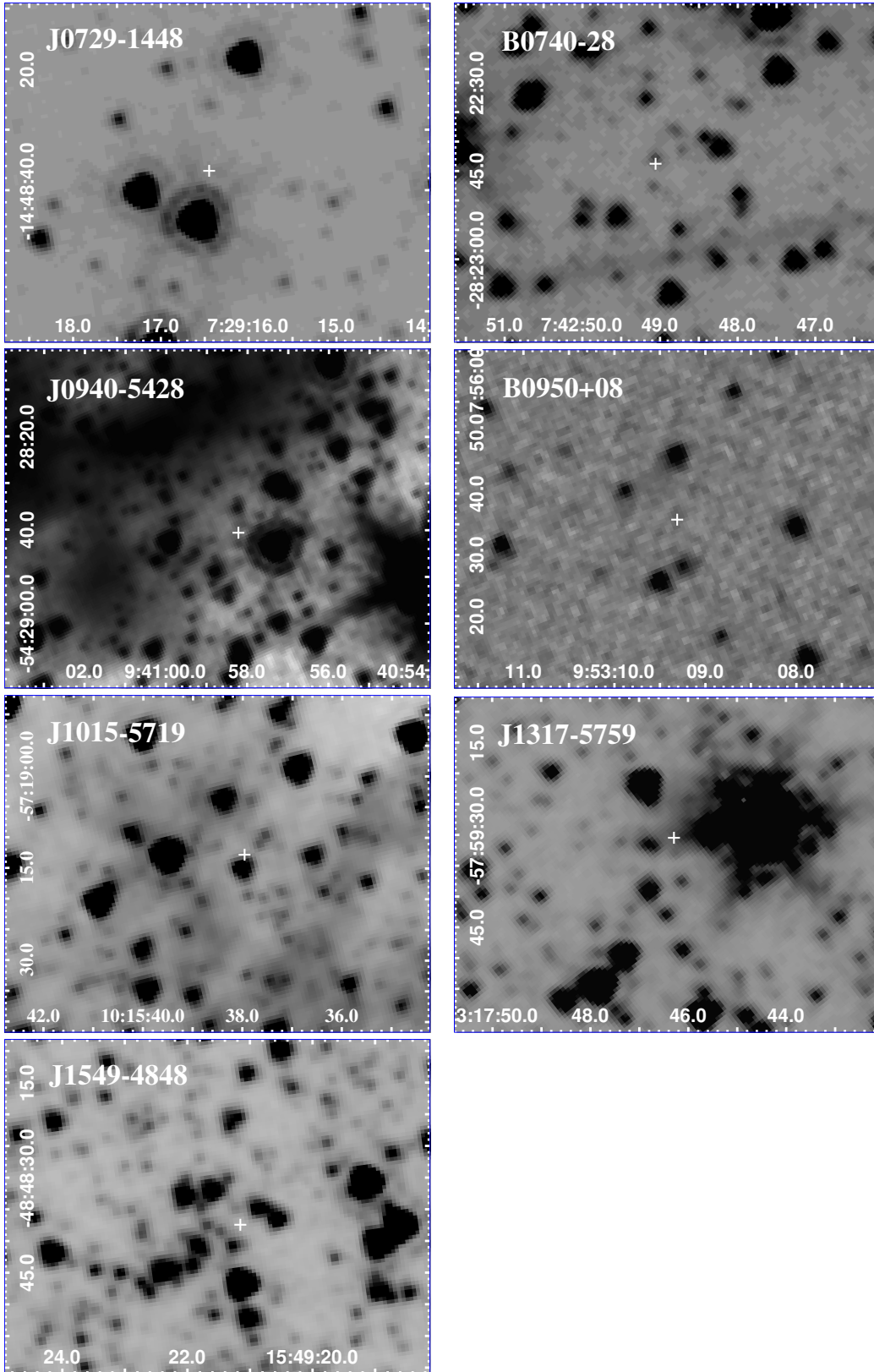


FIG. 1.— *Spitzer*/IRAC 4.5 μ m images of the fields of the seven pulsar targets. The positions of the pulsars are marked by the crosses.

stars were all saturated in our images. The uncertainties are in a range of 0.02–0.06 mag. For B0950+08, only one star with the 2MASS K_s measurement was detected in our image, but the uncertainty is 0.16 mag. Since it was observed in the same night as J0729–1448, the flux calibration results for the latter were used instead.

2.2. *Spitzer* Imaging

The *Spitzer* observations were conducted in the years of 2007–2008, with the observation dates given in Table 2. The imaging instrument used was the Infrared Array Camera (IRAC; Fazio et al. 2004). It operates in four channels at 3.6, 4.5, 5.8, and 8.0 μm . We observed our targets in Channels 2 (4.5 μm) and 4 (8.0 μm). The detectors at the short and long wavelengths are InSb and Si:As devices, respectively, with 256×256 pixels and a plate scale of $1''.2 \text{ pixel}^{-1}$. The field of view (FOV) is $5'.2 \times 5'.2$. To avoid possible saturation caused by bright stars in a target field, the frame times were set to either 12 or 30 s, with 10.4 and 26.8 s effective exposure time per frame, respectively. The total on-source time in each observation is given in Table 2.

The raw image data were processed through the IRAC data pipelines at the *Spitzer* Science Center (SSC). In the Basic Calibrated Data (BCD) pipeline, standard imaging data reductions, such as removal of the electronic bias, dark sky subtraction, flat-fielding, and linearization, were performed and individual flux-calibrated BCD frames were produced. The detailed reduction in the pipelines can be found in the IRAC Instrument Handbook⁷. Using MOPEX, an SSC’s package for reducing and analyzing imaging data, the BCD images were then combined into a final post-BCD (PBCD) mosaic at each channel.

2.3. *WISE* Imaging

Launched on 2009 December 14, *WISE* mapped the entire sky at 3.4, 4.6, 12, and 22 μm (called W1, W2, W3, and W4 bands, respectively) in 2010 with FWHMs of 6.1'', 6.4'', 6.5'', and 12.0'' in the four bands, respectively (see Wright et al. 2010 for details). The *WISE* all-sky images and source catalog were released in 2012 March. We downloaded the *WISE* image data of each source field from the Infrared Processing and Analysis Center (IPAC). The *WISE* observation dates (in year 2010) and the depths of coverage (in units of pixels) are given in Table 2. One pixel of the depth of coverage corresponds to 8.8 s on-source integration time (Wright et al. 2010).

2.4. X-ray Data Analysis

There are pointed X-ray observations for six pulsar targets (except J1549–4848). Among them, only PSRs J0729–1448 and B0950+08 have been detected in X-rays and the results were reported by Kargaltsev & Pavlov (2009) and Zavlin & Pavlov (2004) (see also Becker et al. 2004), respectively. In addition, the X-ray non-detection of PSR J1317–5759 has been reported by McLaughlin (2009).

For the rest of the pulsars, there are archival *XMM-Newton* observations of PSR B0740–28 and *Swift* observations of PSRs J0940–5428 and J1015–5719. PSR

J1549–4848 was only covered by a short exposure in the *ROSAT* All Sky Survey.

We reprocessed the *XMM-Newton* data (ObsID: 0103262401)⁸ of PSR B0740–28 using SAS 13.5.0. After removing periods of high background, we obtained net exposures of 1990 s, 1630 s, and 300 s for MOS1, MOS2, and PN, respectively. The PN data were not included in this analysis, because the exposure is too short to be useful. We combined the MOS1 and MOS2 data but found no detection of the pulsar. Using the CIAO task `aprates`, which is based on a Bayesian algorithm, we obtained a 3σ count rate limit of $7.9 \times 10^{-3} \text{ cts s}^{-1}$ in the 0.5–7 keV energy range.

For PSRs J0940–5428 and J1015–5719, we analyzed the *Swift* data taken in the photon counting mode and processed by the standard pipeline. Three data sets (ObsIDs: 00036695001, 00036695002, and 00036695003) were used for the former with a total exposure of 23.7 ks, and the latter has one 2.8-ks archival exposure (ObsID: 00031631002). No X-ray counterparts were detected. The task `aprates` gives 3σ count rate limits of $5.3 \times 10^{-4} \text{ cts s}^{-1}$ and of $4.5 \times 10^{-3} \text{ cts s}^{-1}$ for PSRs J0940–5428 and J1015–5719, respectively, in the 0.5–7 keV range.

Finally, the *ROSAT* survey image shows no detection for PSR J1549–4848 in X-rays. The exposure of the target field is short, only 330 s.

3. RESULTS

No candidate counterparts to the seven pulsars were detected from IR imaging. The positions of the pulsars in the *Spitzer*/IRAC 4.5 μm images of the fields are shown in Figure 1. For PSR B0740–28, an object is located $0'.88$ north to the pulsar’s position, whose uncertainty is only $0'.05$ determined from long-term pulsar timing (Hobbs et al. 2004). Because the object was also detected in our K_s image, which implies that it is $>5\sigma$ away from the pulsar’s position, it can be excluded as a candidate counterpart. Among the pulsar targets, one IR bow shock was detected around PSR 1549–4848, and studies of the bow shock were reported in Wang et al. (2013).

We estimated 3σ flux upper limits for our ground-based and *Spitzer* imaging by considering that a point source would have been detected if its peak brightness was 3 times larger than the standard deviation of the background counts near a source position. The flux upper limits, particularly for the IRAC observations, are mainly determined by background sky emission and confusion noise when a field is crowded. The obtained flux upper limits are given in Table 2. For *WISE* imaging, images of each source field at the four bands were analyzed and bright *WISE* sources were used for flux calibration. The *WISE* flux upper limits for each pulsar were also estimated, which are given in Table 2. For PSRs J0940–5428 and J1015–5719, large-scale, nebula-like structures were detected around the sources from 4.5 μm to longer wavelength bands (Figure 1), and for PSR J1317–5759, the background emission is high (approximately 10 times higher than that, for example, in the field of B0950+08) and the field is crowded. These

⁷ <http://irsa.ipac.caltech.edu/data/SPITZER/docs/irac/iracinstrumenthandbook/>

⁸ We note that the other observation (ObsID: 0103260501) is not suitable due to severe background flares.

factors resulted in larger flux upper limits than that normally obtained.

The unabsorbed X-ray flux upper limits on PSRs B0740–28, J09404–5428, J1015–5719, and J1549–4848 were also estimated. For PSR B0740–28, we generated the *XMM-Newton* telescope response files with SAS and assumed an absorbed power-law spectrum with photon index of 1.5. The column density was estimated from the pulsar dispersion measure (DM) by assuming 10% ionization (He, Ng, & Kaspi 2013). An unabsorbed flux limit of $1.2 \times 10^{-13} \text{ erg s}^{-1} \text{ cm}^{-2}$ in 0.5–7 keV was obtained. With the same procedure, we obtained $2.9 \times 10^{-14} \text{ erg s}^{-1} \text{ cm}^{-2}$ and $3.2 \times 10^{-13} \text{ erg s}^{-1} \text{ cm}^{-2}$ for PSRs J0940–5428 and J1015–5719, respectively, using the *Swift* telescope response files provided by the calibration team. For PSR 1549–4848, we deduced a 3σ flux upper limit of $4.3 \times 10^{-12} \text{ erg s}^{-1} \text{ cm}^{-2}$ (0.1–2.4 keV) using PIMMS from the count rate limit, which is not very constraining due to the short exposure. The unabsorbed X-ray fluxes or flux upper limits for our pulsar targets are summarized in Table 1.

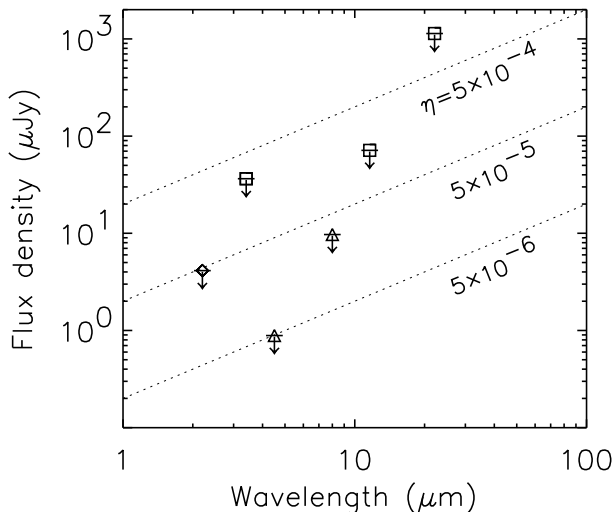


FIG. 2.— Dereddened ground-based K_s (diamond), *Spitzer* (triangles), and *WISE* (squares) flux upper limits of PSR J0729–1448. Different fraction values of L_{sd} are indicated by dotted lines.

4. DISCUSSION

For the pulsar targets, their L_{sd} and d (estimated from their DMs and generally have 30% uncertainties) are listed in Table 1. Except PSR J1317–5759, the pulsars have spin-down fluxes of $7\text{--}90 \times 10^{-11} \text{ erg s}^{-1} \text{ cm}^{-2}$. If a debris disk exists around a pulsar, the energy flux of the pulsar might be intercepted and a fraction of it would be re-radiated by the disk in the IR (e.g., Foster & Fischer 1996). Given that the flux range is within an order of magnitude, we use the first pulsar, PSR J0729–1448, in Table 1 as a main example and discuss the implications from our results.

The extinction A_V to each pulsar target was estimated using the three-dimensional extinction maps of the Galaxy (Drimmel, Cabrera-Lavers, & López-Corredoira 2003). The obtained A_V values are given in Table 1, which are generally consistent with those initially estimated from the Galactic disk dust map (see Section 1.1). In order to obtain the dereddened flux upper limits,

based on which discussions are made below, the reddening laws of Schlegel, Finkbeiner, & Davis (1998) for the near-IR K_s band data, and Indebetouw et al. (2005) (wavelengths $\leq 8 \mu\text{m}$) and Weingartner & Draine (2001) (wavelengths $> 8 \mu\text{m}$) for *Spitzer* and *WISE* data were used.

In Figure 2, the dereddened flux upper limits for PSR J0729–1448 are shown. Assuming that a fraction η of the energy flux from this pulsar would be radiated at the IR bands due to the presence of a dust disk [$\eta(L_{\text{sd}}/4\pi d^2) = \nu F_\nu$, where F_ν is the flux density at a band of frequency ν], the upper limits have reached $\eta \sim 5 \times 10^{-4}$ at $22 \mu\text{m}$. The η value is nearly as deep as that for the planetary system PSR B1257+12 obtained from *Spitzer* MIPS observations (Bryden et al. 2006). However, as pointed out by Bryden et al. (2006), the η limit is still not sufficiently deep since most main-sequence stars with debris disks, which include our solar system, have $\eta < 10^{-5}$. Even if a dust disk exists, emission would not be strong enough to be detected.

At $4.5 \mu\text{m}$, our upper limit has reached $\eta \simeq 5 \times 10^{-6}$. This ratio is at least one order of magnitude deeper than that of the disk case of the magnetar 4U 0142+61, where $(\nu_{4.5\mu} F_{4.5\mu})/F_X \sim 10^{-4}$ (Wang et al. 2007a,b) is used for the comparison because the main energy flux from 4U 0142+61 (as well as 1E 2259+586) is X-ray emission. In Wang et al. (2006), the IR component in the SED of 4U 0142+61 was modelled to arise from a passive, X-ray irradiated disk (see also Vrtilik et al. 1990; Perna et al. 2000), and as the IR-to-X-ray flux ratio $(\nu_{4.5\mu} F_{4.5\mu})/F_X$ might be typical for disks around X-ray bright neutron stars, the flux ratio has been used for the discussion of disk detectability around different young neutron stars (e.g., Wang et al. 2007a,b). Cordes & Shannon (2008) also have proposed that X-ray emission from a neutron star, due to thermal radiation from its high-temperature surface and/or non-thermal radiation from its magnetosphere, provides heating of a debris disk. To check the possibility that a debris disk would be seen mainly due to X-ray heating, we calculated the $(\nu_{4.5\mu} F_{4.5\mu})/F_X$ flux ratio upper limits for PSRs J07294–1448 and B0950+08, which are the only two targets detected with X-ray emission. The ratios are 5.9×10^{-2} and 3.1×10^{-4} , respectively, suggesting that our observations were not sufficiently deep. For the pulsar targets without X-ray detection, the X-ray upper limits of B0740–28, J0940–5428, and J1015–5719 are below or nearly equal to $10^{-3} L_{\text{sd}}$, which is approximately the average fraction of pulsars’ spin-down energy emitted at X-rays (Becker & Truemper 1997; Kargaltsev et al. 2012). The flux limits and fluxes suggest that at least half of our pulsar targets (including PSR J0729–1448) are unfortunately intrinsically faint at X-ray energies.

In this survey of searching for debris disks around neutron stars, we have focused on relatively young radio pulsars with high spin-down fluxes. While only seven such pulsars were observed with the most sensitive IR telescope due to limited, expensive observing time on a space telescope, the results may suggest that it is difficult to detect any debris disks around radio pulsars, whose existence has been hinted by various pieces of indirect evidence. Considering the detections of possible debris disks around two magnetars, another search fo-

cusing on X-ray bright pulsars may be conducted with the future IR telescopes such as the *James-Webb Space Telescope*. Our survey is also limited to relatively hot debris disks, as the stringent sensitivities were provided by *Spitzer* 4.5 and 8.0 μm imaging. In order to complete this survey at multiple wavelengths, searches for cold dust around our pulsar targets should be conducted, given the great capability now available from the Atacama Large Millimeter/submillimeter Array (ALMA) at submillimeter wavelengths. With its sensitivities at least an order of magnitude better than that in the previous searches (e.g., Phillips & Chandler 1994; Löhmer et al. 2004), ALMA observations will help draw a full conclusion about our searches for debris disks around isolated radio pulsars.

This paper includes data gathered with the 6.5 meter Magellan Telescopes located at Las Campanas Observatory, Chile. The work is based in part on observations

made with the *Spitzer* Space Telescope, which is operated by the Jet Propulsion Laboratory, California Institute of Technology under a contract with NASA. The publication makes use of data products from the Wide-field Infrared Survey Explorer, which is a joint project of the University of California, Los Angeles, and the Jet Propulsion Laboratory/California Institute of Technology, funded by NASA.

We thank the anonymous referee for constructive suggestions. This research was supported by the National Natural Science Foundation of China (11373055) and the Strategic Priority Research Program “The Emergence of Cosmological Structures” of the Chinese Academy of Sciences (Grant No. XDB09000000). Z.W. is a Research Fellow of the One-Hundred-Talents project of Chinese Academy of Sciences. A.L. is supported by NSF AST-1311804 and NASA.

Facilities: Magellan (PANIC), *Spitzer* (IRAC)

REFERENCES

- Becker, W., & Truemper, J. 1997, *A&A*, 326, 682
- Becker, W., Weisskopf, M. C., Tennant, A. F., Jessner, A., Dyks, J., Harding, A. K., & Zhang, S. N. 2004, *ApJ*, 615, 908
- Blackman, E. G., & Perna, R. 2004, *ApJ*, 601, L71
- Bryden, G., Beichman, C. A., Rieke, G. H., Stansberry, J. A., Stapelfeldt, K. R., Trilling, D. E., Turner, N. J., & Wolszczan, A. 2006, *ApJ*, 646, 1038
- Çalişkan, S., Ertan, Ü., Alpar, M. A., Trümper, J. E., & Kylafis, N. D. 2013, *MNRAS*, 431, 1136
- Chatterjee, P., Hernquist, L., & Narayan, R. 2000, *ApJ*, 534, 373
- Chevalier, R. A. 1989, *ApJ*, 346, 847
- Cordes, J. M., & Shannon, R. M. 2008, *ApJ*, 682, 1152
- Draine, B. T., & Lee, H. M. 1984, *ApJ*, 285, 89
- Drimmel, R., Cabrera-Lavers, A., & López-Corredoira, M. 2003, *A&A*, 409, 205
- Espinoza, C. M., Lyne, A. G., Kramer, M., Manchester, R. N., & Kaspi, V. M. 2011, *ApJ*, 741, L13
- Farihi, J., Jura, M., & Zuckerman, B. 2009, *ApJ*, 694, 805
- Fazio, G. G., et al. 2004, *ApJS*, 154, 10
- Foster, R. S., & Fischer, J. 1996, *ApJ*, 460, 902
- Gaensler, B. M., & Slane, P. O. 2006, *ARA&A*, 44, 17
- Gotthelf, E. V., Halpern, J. P., & Alford, J. 2013, *ApJ*, 765, 58
- He, C., Ng, C.-Y., & Kaspi, V. M. 2013, *ApJ*, 768, 64
- Hobbs, G., Lyne, A. G., Kramer, M., Martin, C. E., & Jordan, C. 2004, *MNRAS*, 353, 1311
- Indebetouw, R., et al. 2005, *ApJ*, 619, 931
- Jones, P. B. 2007, *MNRAS*, 382, 871
- . 2008, *MNRAS*, 386, 505
- Jura, M., Farihi, J., Zuckerman, B., & Becklin, E. E. 2007, *AJ*, 133, 1927
- Kaplan, D. L., Chakrabarty, D., Wang, Z., & Wachter, S. 2009, *ApJ*, 700, 149
- Kargaltsev, O., Durant, M., Pavlov, G. G., & Garmire, G. 2012, *ApJS*, 201, 37
- Kargaltsev, O., & Pavlov, G. G. 2009, *ApJ*, 702, 433
- Kaspi, V. M., Roberts, M. S. E., & Harding, A. K. 2006, in *Compact stellar X-ray sources*, ed. W. H. G. Lewin & M. van der Klis, 279–339
- Koch-Miramond, L., Haas, M., Pantin, E., Podsiadlowski, P., Naylor, T., & Sauvage, M. 2002, *A&A*, 387, 233
- Lazio, T. J. W., & Fischer, J. 2004, *AJ*, 128, 842
- Lin, D. N. C., Woosley, S. E., & Bodenheimer, P. H. 1991, *Nature*, 353, 827
- Livingstone, M. A., Kaspi, V. M., Gavriil, F. P., Manchester, R. N., Gotthelf, E. V. G., & Kuiper, L. 2007, *Ap&SS*, 308, 317
- Löhmer, O., Wolszczan, A., & Wielebinski, R. 2004, *A&A*, 425, 763
- Manchester, R. N., Hobbs, G. B., Teoh, A., & Hobbs, M. 2005, *AJ*, 129, 1993
- Martini, P., Persson, S. E., Murphy, D. C., Birk, C., Sheckman, S. A., Gunnels, S. M., & Koch, E. 2004, *Proc. SPIE*, 5492, 1653, (astro-ph/0406666)
- McLaughlin, M. 2009, in *Astrophysics and Space Science Library*, Vol. 357, *Astrophysics and Space Science Library*, ed. W. Becker, 41
- McLaughlin, M. A., et al. 2006, *Nature*, 439, 817
- Menou, K., Perna, R., & Hernquist, L. 2001, *ApJ*, 559, 1032
- Michel, F. C., & Dessler, A. J. 1981, *ApJ*, 251, 654
- Miller, M. C., & Hamilton, D. P. 2001, *ApJ*, 550, 863
- Pavlov, G. G., Sanwal, D., & Teter, M. A. 2004, in *IAU Symposium*, Vol. 218, *Young Neutron Stars and Their Environments*, ed. F. Camilo & B. M. Gaensler, 239
- Perna, R., Hernquist, L., & Narayan, R. 2000, *ApJ*, 541, 344
- Phillips, J. A., & Chandler, C. J. 1994, *ApJ*, 420, L83
- Phinney, E. S., & Hansen, B. M. S. 1993, in *Astronomical Society of the Pacific Conference Series*, Vol. 36, *Planets Around Pulsars*, ed. J. A. Phillips, S. E. Thorsett, & S. R. Kulkarni, 371–390
- Qiao, G. J., Xue, Y. Q., Xu, R. X., Wang, H. G., & Xiao, B. W. 2003, *A&A*, 407, L25
- Reach, W. T., Kuchner, M. J., von Hippel, T., Burrows, A., Mullally, F., Kilic, M., & Winget, D. E. 2005, *ApJ*, 635, L161
- Reach, W. T., Lisse, C., von Hippel, T., & Mullally, F. 2009, *ApJ*, 693, 697
- Schlegel, D. J., Finkbeiner, D. P., & Davis, M. 1998, *ApJ*, 500, 525
- Shannon, R. M., et al. 2013, *ApJ*, 766, 5
- Skrutskie, M. F., et al. 2006, *AJ*, 131, 1163
- Thompson, C., & Duncan, R. C. 1996, *ApJ*, 473, 322
- Vrtilek, S. D., Raymond, J. C., Garcia, M. R., Verbunt, F., Hasinger, G., & Kurster, M. 1990, *A&A*, 235, 162
- Wang, Z., Chakrabarty, D., & Kaplan, D. L. 2006, *Nature*, 440, 772
- Wang, Z., Kaplan, D. L., & Chakrabarty, D. 2007a, *ApJ*, 655, 261
- Wang, Z., Kaplan, D. L., Slane, P., Morrell, N., & Kaspi, V. M. 2013, *ApJ*, 769, 122
- Wang, Z., Kaspi, V. M., & Higdon, S. J. U. 2007b, *ApJ*, 665, 1292
- Weingartner, J. C., & Draine, B. T. 2001, *ApJ*, 548, 296
- Wolszczan, A., & Frail, D. A. 1992, *Nature*, 355, 145
- Woods, P. M., & Thompson, C. 2006, *Soft gamma repeaters and anomalous X-ray pulsars: magnetar candidates* (eds. Lewin, W. H. G. and van der Klis, M. (Cambridge: Cambridge Univ. Press)), 547–586
- Woosley, S. E., & Weaver, T. A. 1995, *ApJS*, 101, 181
- Wright, E. L., et al. 2010, *AJ*, 140, 1868
- Xu, S., & Jura, M. 2012, *ApJ*, 745, 88
- Zavlin, V. E., & Pavlov, G. G. 2004, *ApJ*, 616, 452

TABLE 1
PROPERTIES AND DERIVED FLUXES OR FLUX UPPER LIMITS FOR THE SEVEN RADIO PULSAR TARGETS

Pulsar	Age (kyr)	d (kpc)	Gb (deg)	$L_{\text{sd}}/10^{35}$ (erg s $^{-1}$)	$F_X^a/10^{-14}$ (erg s $^{-1}$ cm $^{-2}$)	A_V (mag)	$F_{4.5\mu}^b$ (μJy)	$(\nu_{4.5\mu} F_{4.5\mu})/F_X$
J0729–1448	35	4.4	+1.4	2.8	1.0	1.1	<0.87	< 5.9×10^{-2}
B0740–28	160	1.9	–2.4	1.4	<12	0.93	<0.061	...
J0940–5428	40	4.3	–1.3	19	<2.9	4.1	<1.6	...
B0950+08	10 4	0.26	+43.7	0.006	12	0.088	<0.056	< 3.1×10^{-4}
J1015–5719	40	4.9	–0.6	8.3	<32	5.3	<0.79	...
J1317–5759	10 3	5.6	+4.7	0.002	<74	2.2	<16	...
J1549–4848	300	1.5	+4.3	0.2	<430	1.6	<0.41	...

^a X-ray flux is unabsorbed. The energy range for J0729–1448 is 0.5–8 keV, for B0740–28, J0940–5428, and J1015–5719 is 0.5–7 keV, for B0950+08 is 0.2–10 keV, for J1317–5759 is 0.3–5 keV, and for J1549–4848 is 0.1–2.4 keV.

^b Dereddened flux upper limits at the *Spitzer* IRAC channel 2.

TABLE 2
OBSERVATIONS OF SEVEN RADIO PULSAR TARGETS

	J0729–1448	B0740–28	J0940–5428	B0950+08	J1015–5719	J1317–5759	J1549–4848
Magellan/PANIC							
Obs. date	2006/05/15	2005/10/22	2006/05/16	2006/05/15	2006/05/16	2006/05/16	2006/05/17
Exposure (min)	22.5	13.5	22.5	30.0	22.5	30.0	22.5
FWHM (arcsec)	0.56	0.43	0.40	0.46	0.39	0.49	0.40
K_s flux limit (mag)	20.7	21.2	20.7	20.7	20.4	21.0	21.2
Spitzer/IRAC							
Obs. date	2007/11/14	2008/01/01	2008/04/08	2007/12/27	2008/04/08	2007/09/12	2007/09/12
Exposure (min)	17.9	17.9	17.3	17.9	17.9	17.3	17.9
Ch2 flux limit (μJy)	0.82	0.058	1.3	0.056	0.61	14	0.38
Ch4 flux limit (μJy)	9.1	6.9	89	6.4	140	15	1.4
WISE							
Obs. date	2010/04/10	2010/04/16	2010/06/14	2010/05/11	2010/01/07	2010/01/31	2010/02/22
	2010/07/05	2010/08/04	...
Depth of coverage (pixel)	14	14	32	12	34	34	14
W1 flux limit (μJy)	33	61	160	170	140	94	85
W2 flux limit (μJy)	20	34	87	37	110	27	56
W3 flux limit (μJy)	67	92	250	89	880	72	140
W4 flux limit (μJy)	1100	1100	5400	1300	5100	750	790